Enhanced transmission through metallic plates perforated by arrays of subwavelength holes and sandwiched between dielectric slabs

Vitaliy Lomakin* and Eric Michielssen
Center for Computational Electromagnetics, University of Illinois at Urbana-Champaign, Urbana, Illinois 61801, USA
(Received 20 September 2004; revised manuscript received 11 December 2004; published 29 June 2005)

This paper presents analytical and numerical studies demonstrating that a perfectly conducting metallic plate perforated by a periodic array of subwavelength holes and sandwiched in between two dielectric slabs permits enhanced transmission of electromagnetic plane waves in both the optical and microwave regimes, and this for both transverse magnetically and electrically polarized fields. The enhanced transmission mechanism is attributed to coupling between the incident plane wave and resonances supported by the perforated plate that are associated with the existence of grounded dielectric slab guided waves. The enhanced transmission phenomenon occurs in one of two regimes. In the single resonance regime, the incident plane wave couples to a resonance supported by only a single slab. The transmission coefficient magnitude peaks as the excitation frequency scans through the resonance; however, the peak magnitude decays exponentially with plate thickness. In the double resonance regime, the incident plane wave couples to resonances in both slabs simultaneously. The transmission coefficient magnitude exhibits twin peaks whose magnitudes typically are larger than those resulting from single resonances and that remain large even for plates of moderate thickness. It is demonstrated that double resonances may occur for symmetric as well as for asymmetric structures, i.e., when the two slabs are identical or different. For symmetric structures double resonances occur for any angle of incidence. In contrast, for asymmetric structures, special conditions on the period and slab parameters have to be satisfied for the structure to support one or more double resonances.

DOI: 10.1103/PhysRevB.71.235117 PACS number(s): 42.25.Fx, 42.79.Dj, 42.79.Ag, 78.67.−n

I. INTRODUCTION

Metal plates perforated by subwavelength holes find numerous uses in physics and engineering including the construction of probes for imaging and microscopy,[1] the synthesis of microwave and optical filters,[2] and the manufacturing of cost-effective ground planes and electromagnetic shields.[3] Classical Bethe theory[4] predicts that electromagnetic power transmitted through an infinitesimally thin perfect electrically conducting (PEC) plate perforated by noninteracting holes of subwavelength size is very weak and scales as $(s/\lambda)^4$ when normalized to the hole area; here λ is the wavelength of the illumination and s is the hole size. However, the transmitted power may be enhanced substantially when the holes interact resonantly. Indeed, a recent experiment by Ebbesen demonstrated that *optical* power incident on a metal plate perforated by an appropriately dimensioned periodic array of subwavelength holes largely may be transmitted, this seemingly in defiance of Bethe's theory.[5] Ebbesen's discovery catalyzed many experimental and theoretical studies into optical *enhanced transmission* phenomena.[6–19] Many of these studies' authors attribute optical enhanced transmission phenomena to resonant coupling of the incident plane wave to surface plasmon polaritons (SPPs—surface waves supported by metal surfaces with a negative permittivity); strong coupling is said to occur when the transverse wavenumber of one of the Floquet modes generated by the interaction of the incident wave with the perforated plate matches that of the SPP.[6–10,12–20] This viewpoint also leads to the recognition that *optical* enhanced transmission through arrayed holes in metal plates occurs either in a *single* or in a *double resonance* regime.[12–14,21] *Single resonances* occur when a field bound to either the bottom *or* top face of the perforated plate strongly participates in transmission enhancement. *Double resonances* occur when field bound to both plate faces simultaneously participate in the transmission enhancement; the ensuing transmission enhancement typically is stronger than that associated with single resonances. Most studies to date have associated double resonances with structures that are symmetric with respect to the plate center.[12,13,21] One study suggested that double resonance enhanced transmission can be achieved through asymmetric modulated metallic plates,[14] though no results demonstrating the effect were presented. In a departure from the above SPP-centered approaches, Treacy[11] presents a unified explanation of enhanced transmission phenomena using dynamic diffraction concepts; contrary to the above referenced works, he does not assign a causative role to SPPs but rather explains these phenomena in terms of modal solutions of Maxwell's equations thus allowing for a host of different physical mechanisms to be modeled within the same framework. Treacy[11] applies his technique to the study of enhanced transmission phenomena occurring on metal plates with subwavelength slits.[22–25] It is to be noted, however, that unlike holes with simply connected cross sections, slits support transverse electric and magnetic (TEM) modes; therefore the transmission properties of metal plates with slits differ from those of metal plates with holes.

Phenomena of enhanced plane wave transmission through arrayed holes in metal plates are manifestations of so-called resonant Wood anomalies.[15,26] Mathematically, resonant Wood anomalies manifest themselves through the presence of complex frequency (angular) poles in the scattering coefficient of the periodic grating for a given real incident angle

(frequency). When the incident plane wave frequency (angle) is scanned near these poles, rapid variations and/or peaks in the scattering coefficient are observed. Resonant Wood anomalies may occur on any metal-dielectric plate that supports a slow wave when loaded by an appropriate periodic grating. It should come as no surprise that recently several non-SPP mechanisms leading to *optical and microwave* enhanced transmission through metallic plates perforated by subwavelength holes have been identified.[13,21,27–33] These mechanisms all involve coupling of incident fields to resonances existing on periodic arrays and associated with the slow waves they support. Unfortunately, the above (and many more unreferenced) studies notwithstanding, our present understanding of enhanced transmission phenomena on metal plates is incomplete. The present catalog of enhanced transmission mechanisms and the structures that support them do not provide scientists and engineers the design freedom and control needed in many practical applications. Many interesting structures that (may) support tunable enhancement mechanisms remain unexplored.

This paper presents analytical and numerical studies of phenomena of enhanced transmission of transverse magnetic (TM) and transverse electric (TE) polarized plane waves through PEC plates sandwiched in between two dielectric slabs and perforated by a doubly periodic array of subwavelength holes. It should be noted that this structure has been studied and used extensively in the past.[34,35] However, for plates perforated by subwavelength holes, the transmitted field was presumed to be very weak and no enhanced transmission phenomena were reported (except for our recent conference report).[36] This paper's contributions are twofold. First, the paper demonstrates, via analytical and numerical means, that the suggested structure, viz. a metal plate perforated by an array of subwavelength holes that is sandwiched in between two (potentially different) dielectric slabs, may give rise to enhanced transmission phenomena, even in the microwave regime where metals are safely modeled as (lossy or lossless) electric conductors that do not support SPPs. Moreover, it is shown that the structure allows enhanced transmission of arbitrarily (TE and TM) polarized fields and permits tuning of the enhanced transmission resonant frequency, resonance bandwidth, and polarization by varying its construction parameters. Second, the paper presents a theoretical analysis of the enhanced transmission mechanisms in both the single and double resonance regimes. The latter is explored for both symmetric and asymmetric configurations, viz. for identical and different bottom and top slabs, and changes in the nature of the phenomenon induced by increases in plate thickness are explored. It is noted that this particular structure supports phenomena representative of those occurring on many other subwavelength hole structures including metal perforated plates whose surfaces support other types of (identical or different) slow waves.

II. PROBLEM FORMULATION

Consider a PEC plate of thickness d that is perforated by a doubly periodic orthogonal array of circular holes of radius $s \ll \lambda$ (Fig. 1). The array's principal axes extend along the x and y directions with periodicities L_x and L_y, respectively. The plate is sandwiched in between two dielectric slabs of thicknesses and relative permittivities h_i and ε_i with $i=1$ (bottom) or 2 (top). The center of the PEC plate resides at $z=0$ and the structure is excited from below by a TM or TE plane wave with magnetic/electric field $\hat{\mathbf{y}}e^{-jk_0[\xi x+(1-\xi^2)^{1/2}z]}$; here $k_0=2\pi/\lambda=2\pi f/c$ is the free-space wave number with f as the frequency and c as the free-space speed of light. In addition, $\xi=\sin\theta^i$ is the incident field's normalized transverse wave number with θ^i the incidence angle. Throughout this paper, an $e^{j\omega t}$ time dependence is suppressed. Furthermore, it is assumed that $h_i<(\varepsilon_i-1)^{-1/2}\lambda/2$, $i=1,2$ to guarantee that, for a given polarization and in the absence of holes, i.e., when $s=0$, the structure supports at most one guided wave (GW) in each of the dielectric slabs.[37] The above excitation, upon interacting with the perforated plate, produces a scattered field that can be expressed as a sum of Floquet (diffraction) modes. It is assumed that $2s<L_y \ll \lambda$ and $L_x<\lambda/2$; these conditions guarantee that the scattered field comprises only one propagating Floquet mode and thus that the magnetic/electric field for sufficiently large $z>d/2+h_2$ can be expressed as $\hat{\mathbf{y}}T(f)e^{-jk_0[\xi x+(1-\xi^2)^{1/2}z]}$ where $T(f)$ is the *zeroth-order transmission coefficient*. Other consequences of the above restrictions on L_x and L_y are elucidated below. It is noted, however, that all restrictions on L_x and L_y are introduced solely to render our discussions more transparent and that they can be removed without affecting the nature of the enhanced transmission phenomena studied.

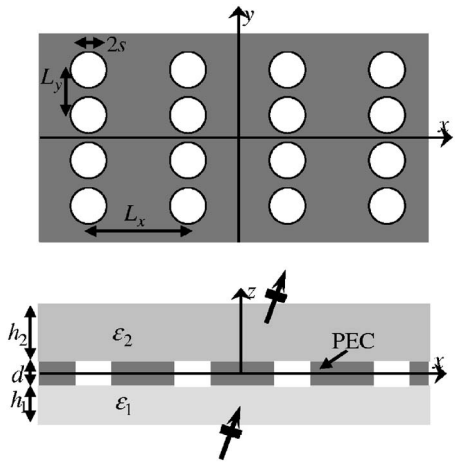

FIG. 1. Problem configuration.

III. MODEL OF TRANSMISSION COEFFICIENT $T(f)$

In the absence of holes the two grounded slabs in the structure of Fig. 1 support TM/TE GWs[37] with frequency-dependent and real-valued normalized transverse wavenumbers $\xi_{gw}^{(i)}(f)$ $(i=1,2)$, satisfying

$$\begin{cases} \varepsilon_i k_{z0} + jk_{z0}^{(i)} \tan(k_{z0}^{(i)} h_i) = 0 & \text{for TM polarization,} \\ k_{z0}^{(i)} + jk_{z0} \tan(k_{z0}^{(i)} h_i) = 0 & \text{for TE polarization,} \end{cases}$$

$$k_{z0} = k_0\sqrt{1-[\xi_{gw}^{(i)}(f)]^2}, \quad k_{z0}^{(i)} = k_0\sqrt{\varepsilon_i - [\xi_{gw}^{(i)}(f)]^2}; \quad i = 1,2. \tag{1}$$

It can be shown that $1 < |\xi_{gw}^{(i)}(f)| < \max_i\{\varepsilon_i^{1/2}\}$. When $s \neq 0$, the structure supports source-free fields that can be represented as an infinite series of cross-coupled Floquet (diffraction) modes via $\Sigma_{l_x,l_y=-\infty}^{\infty} a_{l_x,l_y}(z)e^{-j2\pi\xi x f_{p,n}^{(i)}/c - j2\pi l_x x/L_x - j2\pi l_y y/L_y}$; here l_x, l_y are Floquet mode indices, $a_{l_x,l_y}(z)$ are modal amplitudes, and $f_{p,n}^{(i)}$ are (complex) characteristic frequencies. Since $|\xi| < 1$ and $s, L_y \ll \lambda$, the characteristic frequencies approximately satisfy $f_{p,n}^{(i)} \approx f_{r,n}^{(i)}$, where the (real) resonant frequencies $f_{r,n}^{(i)}$ solve $\xi = \mathrm{sign}(n)\xi_{gw}(f_{r,n}) - (cn)/(f_{r,n}L_x)$, i.e.,

$$f_{r,n}^{(i)} = \frac{nc}{\{\mathrm{sign}(n)|\xi_{gw}^{(i)}(f_{r,n}^{(i)})| - \xi\}L_x}. \tag{2}$$

The source-free solutions associated with the lowest order frequencies $f_{p,\pm1}^{(i)}$ exhibit strong coupling between the $\pm$ first-order ($l_x = \pm 1, l_y = 0$) and the zeroth-order ($l_x = l_y = 0$) Floquet modes. Whereas the zeroth-order Floquet mode dominates the source-free field away from the perforated plate, the $\pm$ first-order Floquet modes constitute perturbations of grounded slab GWs propagating along the positive (+1) and negative (−1) x directions and dominate the source-free field near the perforated plate. Note also that, due to the TE GW cutoff phenomenon, TE enhanced transmission only will occur when at least one slab has sufficiently large electrical thickness, that is when $h_i > (\varepsilon_i - 1)^{-1/2}\lambda/4$, for $i = 1$ and/or 2.[37]

The incident plane wave couples to the source-free fields (resonances) when $f \approx f_{r,n}^{(i)} \approx \mathrm{Re}\{f_{p,n}^{(i)}\}$ (note that a resonance can only be excited by an incident field with a frequency spectrum with nonvanishing support; therefore, here the term "coupling" refers to the fact that the scattered field is strongly affected by the presence of resonances). As a manifestation of this coupling the frequencies $f_{p,n}^{(i)}$ appear as poles to $T(f)$. In other words, $T(f)$ can be expressed as

$$T(f) = \sum_{n,i} \frac{\mathrm{Res}\{T(f_{p,n}^{(i)})\}}{f - f_{p,n}^{(i)}} + a(f). \tag{3}$$

The first and second terms in (3) model $T(f)$'s resonant and nonresonant components. The resonant component is characterized by complex poles $f_{p,n}^{(i)}$, which describe the resonances occurring on the structure, and the corresponding residues $\mathrm{Res}\{T(f_{p,n}^{(i)})\}$, which quantify the excitation of these resonances by the incident plane wave. The nonresonant component $a(f)$ is smooth and weaker than the resonant one for f near all $\mathrm{Re}\{f_{p,n}^{(i)}\}$.[38]

As a precursor to a study of $|T(f)|$ for various structure parameters (presented in Secs. IV and V), the dispersion of the lowest-order poles $f_{p,\pm1}^{(i)}$ and their residues with respect to positive ξ is studied. The poles were obtained using the modal approach detailed in Refs. 34 and 35. The perforated plate parameters are $L_x = 26$ mm, $L_y = 5$ mm, $s = 2.4$ mm, and $d = 2.5$ mm; the plate is sandwiched in between two different slabs with $\varepsilon_1 = 3$, $h_1 = 3$ mm and $\varepsilon_2 = 3$, $h_2 = 8$ mm. The incident field normalized wavenumber is varied in the range $0 < \xi < 0.25$ These parameters were selected as they lead to "typical dispersion diagrams." Figures 2(a) and 2(b) track $\mathrm{Re}\{f_{p,\pm1}^{(i)}\}$ and $\mathrm{Im}\{f_{p,\pm1}^{(i)}\}$ of TM and TE poles in the first two passbands. In addition, Fig. 2(a) tracks $f_{r,\pm1}^{(i)}$ and Fig. 2(b) tracks $|\mathrm{Res}\{T(f_{p,\pm1}^{(i)})\}|$. Four TM poles $f_{p,\pm1}^{(1,2)}$ and two TE poles $f_{p,\pm1}^{(2)}$ are obtained; no TE poles exist for $|n| = i = 1$ as then Eqs. (1) and (2) have no real solution due to the TE cutoff phenomenon. All the poles $f_{p,\pm1}^{(i)}$ reside near the corresponding resonant frequencies $f_{r,\pm1}^{(i)}$ since $\mathrm{Re}\{f_{p,\pm1}^{(i)}\} \approx f_{r,\pm1}^{(i)}$ and $\mathrm{Im}\{f_{p,\pm1}^{(i)}\} \ll \mathrm{Re}\{f_{p,\pm1}^{(i)}\}$. Several observations regarding the structure of these dispersion diagrams are in order.

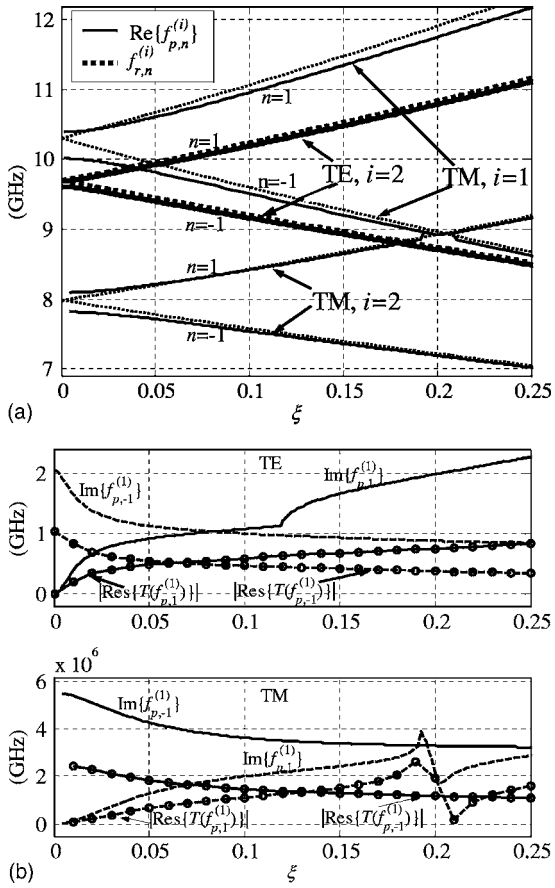

FIG. 2. Dispersion graphs for the structure with $L_x = 26$ mm, $L_y = 5$ mm, $s = 2.4$ mm, $\varepsilon_1 = 3$, $h_1 = 3$ mm and $\varepsilon_2 = 3$, $h_2 = 8$ mm for TM and TE polarization. (a) tracks $\mathrm{Re}\{f_{p,\pm1}^{(1,2)}\}$; (b) tracks $\mathrm{Im}\{f_{p,\pm1}^{(1,2)}\}$ and $|\mathrm{Res}\{f_{p,\pm1}^{(1,2)}\}|$.

(i) First, it is observed that all pole trajectories delineate stopbands for broadside excitations, viz. $\xi = 0$. Furthermore, it is found that $\mathrm{Im}\{f_{p,1}^{(i)}\} \to 0$, $\mathrm{Res}\{T(f_{p,1}^{(i)})\} \to 0$ as $\xi \to 0$. Physically, this is because when $\xi \to 0$ both the $\pm$ first Floquet modes strongly couple to the incident plane wave. This results in two possible standing waves whose y and z directed electric field components are symmetric or antisymmetric with respect to the $x = 0$ plane. However, since the structure in Fig. 1 is symmetric with respect to $x = 0$, only the symmetric standing wave can be excited.

(ii) Second, it is noted that for most ξ, poles $f_{p,\tilde{n}}^{(1)}$ and $f_{p,\tilde{n}'}^{(2)}$ associated with GWs in the bottom and top slabs coupling to identical (for $\tilde{n} = \tilde{n}'$) or different (for $\tilde{n} \neq \tilde{n}'$) Floquet modes

are *well-separated* (example: poles $f_{p,1}^{(1)}$ and $f_{p,-1}^{(2)}$ for the TM polarization; the notion of pole separation is quantified in Sec. IV). In other words, for most ξ, the resonances described by poles $f_{p,\tilde{n}}^{(1)}$ and $f_{p,\tilde{n}'}^{(2)}$ are uncoupled. When a pole $f_{p,\tilde{n}}^{(\tilde{i})}$ is well separated from all others, it gives rise to *single-resonance enhanced transmission*. Under certain conditions, however, poles $f_{p,\tilde{n}}^{(1)}$ and $f_{p,\tilde{n}'}^{(2)}$ may reside near one another (example: poles $f_{p,-1}^{(1)}$ and $f_{p,1}^{(2)}$ for the TM polarization near $\xi=0.2005$, where the trajectories of $\mathrm{Re}\{f_{p,-1}^{(1)}\}$ and $\mathrm{Re}\{f_{p,1}^{(2)}\}$ intersect and $\mathrm{Im}\{f_{p,-1}^{(1)}\}$ and $\mathrm{Im}\{f_{p,1}^{(2)}\}$ experience rapid variations). When this happens, the resonances in the bottom and top slabs described by poles $f_{p,\tilde{n}}^{(1)}$ and $f_{p,\tilde{n}'}^{(2)}$ couple, resulting in *double resonance enhanced transmission*. These distinct enhanced transmission phenomena are discussed in the next two sections.

IV. SINGLE RESONANCE ENHANCED TRANSMISSION

Consider a pole $f_{p,\tilde{n}}^{(\tilde{i})}$ which, for a given ξ, is well separated from all other poles. This implies that for $f \approx \mathrm{Re}\{f_{p,\tilde{n}}^{(\tilde{i})}\}$ enhanced transmission is observed due to a resonance occurring only in a *single* (top or bottom) slab; note that there also exists a weak coupling between the fields in the top and bottom slabs. It follows that for $f \approx \mathrm{Re}\{f_{p,\tilde{n}}^{(\tilde{i})}\}$ the resonant component of $T(f)$ in essence is due to $f_{p,\tilde{n}}^{(\tilde{i})}$; hence, $T(f)$ can be expressed as

$$T(f) = \frac{\mathrm{Res}\{T(f_{p,\tilde{n}}^{(\tilde{i})})\}}{f - f_{p,\tilde{n}}^{(\tilde{i})}} + \tilde{a}(f) = \frac{f - f_{z,\tilde{n}}^{(\tilde{i})}}{f - f_{p,\tilde{n}}^{(\tilde{i})}} \tilde{b}(f). \tag{4}$$

From (4) it follows that, for $f \approx \mathrm{Re}\{f_{p,\tilde{n}}^{(\tilde{i})}\}$ the graph of $|T(f)|$ vs f is comprised of a *single* enhanced transmission peak whose location and bandwidth are determined by $\mathrm{Re}\{f_{p,\tilde{n}}^{(\tilde{i})}\}$ and $[\mathrm{Im}\{f_{p,\tilde{n}}^{(\tilde{i})}\}]^{-1}$, respectively. The nonresonant component $\tilde{a}(f)$ includes $a(f)$ and contributions from all poles $f_{p,n}^{(i)}$ with $n \neq \tilde{n}, i \neq \tilde{i}$; these contributions are weak as the poles are far removed from $f_{p,\tilde{n}}^{(\tilde{i})}$. Equation (4) and its interpretation are valid for $|f - \mathrm{Re}\{f_{p,\tilde{n}}^{(\tilde{i})}\}| < \chi\, \mathrm{Im}\{f_{p,\tilde{n}}^{(\tilde{i})}\}$ provided that $|\mathrm{Re}\{f_{p,n}^{(i)} - f_{p,\tilde{n}}^{(\tilde{i})}\}| > \chi\, \mathrm{Im}\{f_{p,n}^{(i)} + f_{p,\tilde{n}}^{(\tilde{i})}\}$ for all $n \neq \tilde{n}, i \neq \tilde{i}$; here $\chi > 1$ is a dimensionless factor determined by the desired adequacy of model (4) and the magnitude of the nonresonant component. Approximating $\tilde{a}(f) \approx \tilde{a}(f_{p,\tilde{n}}^{(\tilde{i})})$ and combining it with the resonant contribution leads to $T(f) \approx a(f_{p,\tilde{n}}^{(\tilde{i})})[f - f_{p,\tilde{n}}^{(\tilde{i})} + \mathrm{Res}\{T(f_{p,\tilde{n}}^{(\tilde{i})})\}/a(f_{p,\tilde{n}}^{(\tilde{i})})]/[f - f_{p,\tilde{n}}^{(\tilde{i})}]$. As a result, $T(f)$ has a simple zero $f_{z,\tilde{n}}^{(\tilde{i})} \approx f_{p,\tilde{n}}^{(\tilde{i})} - \mathrm{Res}\{T(f_{p,\tilde{n}}^{(\tilde{i})})\}/a(f_{p,\tilde{n}}^{(\tilde{i})})$ and $T(f)$ can be expressed as in the second equality of (4) with $b(f) \approx \tilde{a}(f) \approx \tilde{a}(f_{p,\tilde{n}}^{(\tilde{i})})$. The zero $f_{z,\tilde{n}}^{(\tilde{i})}$ is located near the pole $f_{p,\tilde{n}}^{(\tilde{i})}$ provided that $|\mathrm{Res}\{T(f_{p,\tilde{n}}^{(\tilde{i})})\}/a(f_{p,\tilde{n}}^{(\tilde{i})})|$ is not too small—a condition that in practice almost always is satisfied. As a consequence, for f near $\mathrm{Re}\{f_{p,\tilde{n}}^{(\tilde{i})}\}$, the graph of $|T(f)|$ vs f typically has an *asymmetric* profile with a maximum accompanied by a deep minimum. Note that such $|T(f)|$ profiles often are observed when studying scattering coefficients of periodic gratings, including plates with subwavelength holes, and that they have been associated with resonant Wood anomalies in the past.[15,26]

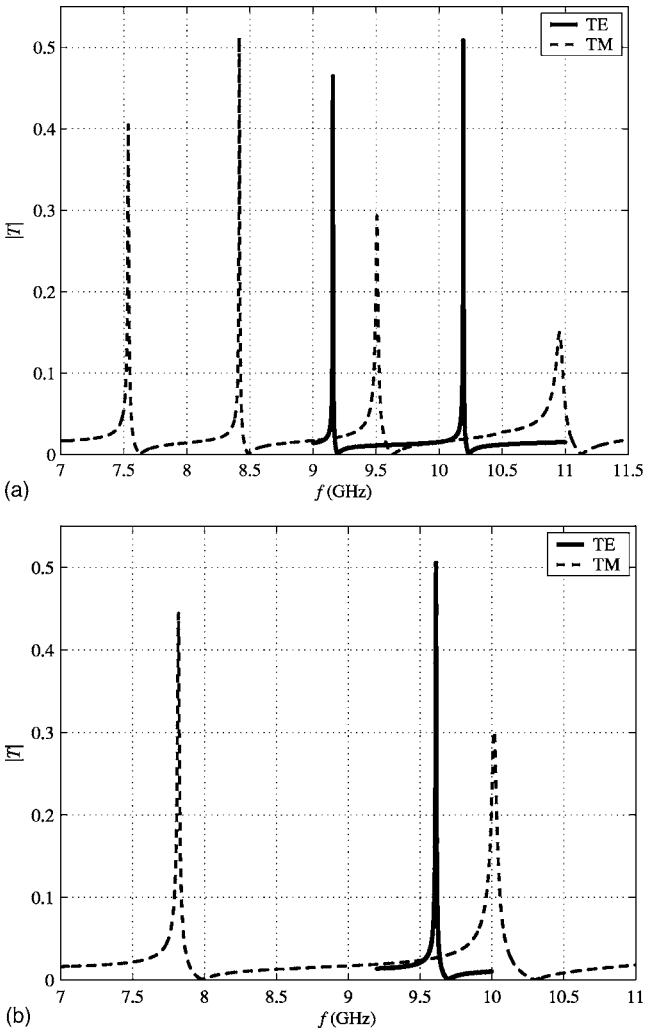

FIG. 3. Magnitude of TM and TE transmission coefficient through the structures in Fig. 2 for (a) off-normal incidence $\xi=0.1$ and (b) normal incidence $\xi=0$.

To illustrate the validity of the above model, scattering from the structure detailed in Sec. III illuminated by plane waves with various angles of incidence, polarizations, and frequencies, was analyzed.

Figures 3(a) and 3(b) depict $|T(f)|$ for incident plane waves with $\xi=0.1$ and $\xi=0$, respectively. Both the TM and TE polarizations are analyzed and the frequency range considered includes $\mathrm{Re}\{f_{p,n}^{(i)}\}$ for all poles considered in Fig. 2. For off-normal incidence ($\xi=0.1$), four TM and two TE single resonance enhanced transmission peaks are observed. For normal incidence ($\xi=0$), only two TM single resonance peaks and one TE single resonance peak survive. The number of peaks equals the number of excited poles and their

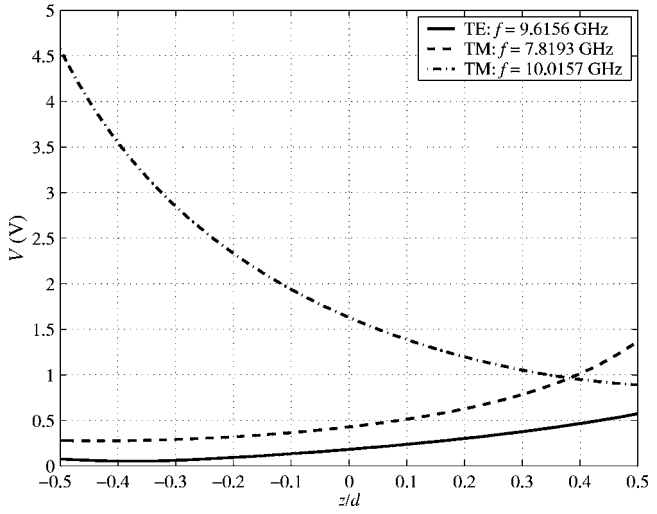

FIG. 4. Function $V(z/d)=[\int_{\text{area}}^{\text{hole}}(|E_x|^2+|E_y|^2)dxdy]^{1/2}$ characterizing the tangential field inside the holes under TE plane wave excitation. The structure parameters are as in Fig. 2 with $\xi=0$ and $d=1.5$ mm.

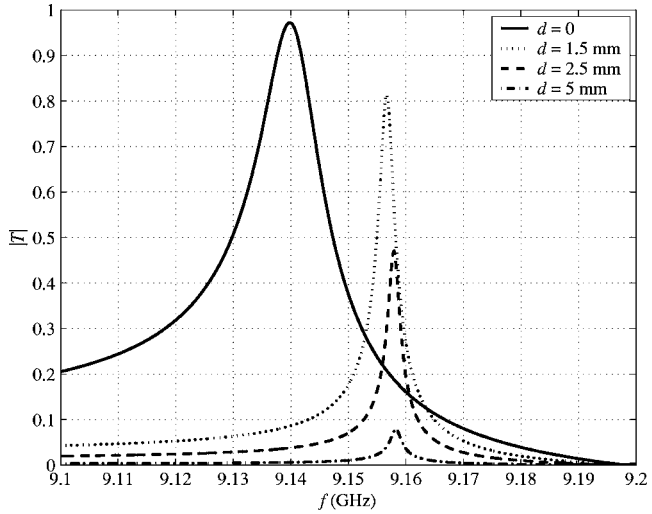

FIG. 5. Magnitude of TE transmission coefficient through the structures in Fig. 2 for $\xi=0.1$ and different d.

location is very near those of the corresponding $\text{Re}\{f_{p,n}^{(i)}\}$ shown in Fig. 2(a). Moreover, the peaks have asymmetric profiles with maxima and deep minima as predicted by (4).

To pin down the origins of the enhanced transmission phenomena for $\xi=0$, Fig. 4 displays the function $V(z/d)=[\int_{\text{area}}^{\text{hole}}(|E_x|^2+|E_y|^2)dxdy]^{1/2}$ for the three frequencies f at which $|T(f)|$ in Fig. 3(b) peaks. For the TM polarization, the function $V(z/d)$ reaches its maximum at $z=d/2$ and $z=-d/2$ for the peaks associated with poles $f_{p,-1}^{(2)}$ and $f_{p,-1}^{(1)}$, respectively. Moreover, for z away from those maxima the function $V(z/d)$ *decays exponentially*. This demonstrates that the resonances associated with poles $f_{p,-1}^{(2)}$ and $f_{p,-1}^{(1)}$ indeed occur in the top and bottom slabs, respectively. For the TE polarization, the field is greatest at $z=d/2$, demonstrating that it results from a resonance in the top slab associated with the pole $f_{p,-1}^{(2)}$.

To elucidate the dependence of single resonance enhanced transmission phenomena on the plate thickness d, Fig. 5 tracks $|T(f)|$ versus frequency for a TE polarized field with $\xi=0.1$ incident on a structure that is identical to that studied in Sec. III except for the plate thickness d, which is varied. It is observed that, although the largest enhanced transmission peak is obtained for $d=0$, total transmission is never obtained. Furthermore, as d increases the transmission peak narrows, moves towards higher frequencies, and decreases exponentially in magnitude. This behavior is due to the fact that coupling between the bottom and top plate faces too reduces exponentially with plate thickness.

V. DOUBLE RESONANCE ENHANCED TRANSMISSION

Consider a slab configuration, angle of incidence, and polarization for which the resonant frequencies $f_{r,\tilde{n}}^{(1)}$ and $f_{r,\tilde{n}'}^{(2)}$ coincide. It follows from the discussion in Section III that the poles $f_{p,\tilde{n}}^{(1)}$ and $f_{p,\tilde{n}'}^{(2)}$ reside close to one another, too. This implies that for $f\approx\text{Re}\{f_{p,\{\tilde{n},\tilde{n}'\}}^{(\{1,2\})}\}$ enhanced transmission arises due to a composite resonance resulting from not only (*horizontal*) interactions between Floquet modes, but also strong (*vertical*) interactions between fields in the bottom and top slabs. In this situation the superscript index in $f_{p,\tilde{n}}^{(1)}$ and $f_{p,\tilde{n}'}^{(2)}$ only has a nomenclature function as it no longer points to a resonance in a particular slab; in practice we label the two poles such that $\text{Re}\{f_{p,\tilde{n}}^{(1)}\}<\text{Re}\{f_{p,\tilde{n}'}^{(2)}\}$. By repeating the arguments leading to (4) but retaining two poles in the resonant component of (3), $T(f)$ for $f\approx\text{Re}\{f_{p,\{\tilde{n},\tilde{n}'\}}^{(\{1,2\})}\}$ is modeled as

$$T(f)=\frac{\text{Res}\{T(f_{p,\tilde{n}}^{(1)})\}}{f-f_{p,\tilde{n}}^{(1)}}+\frac{\text{Res}\{T(f_{p,\tilde{n}'}^{(2)})\}}{f-f_{p,\tilde{n}'}^{(1)}}+\tilde{a}(f)$$
$$=\frac{[f-f_{z,\tilde{n}}^{(1)}][f-f_{z,\tilde{n}'}^{(2)}]}{[f-f_{p,\tilde{n}}^{(1)}][f-f_{p,\tilde{n}'}^{(2)}]}\tilde{b}(f). \quad (5)$$

From (5) it follows that, for $f\approx\text{Re}\{f_{p,\{\tilde{n},\tilde{n}'\}}^{(\{1,2\})}\}$, the graph of $|T(f)|$ vs f exhibits *two* enhanced transmission peaks with locations and resonance bandwidths determined by $\text{Re}\{f_{p,\{\tilde{n},\tilde{n}'\}}^{(1,2)}\}$ and $[\text{Im}\{f_{p,\{\tilde{n},\tilde{n}'\}}^{(1,2)}\}]^{-1}$, respectively. Equation (5) is valid for $|\min_{i=1,2,n=\tilde{n},\tilde{n}'}\{f-\text{Re}\{f_{p,n}^{(i)}\}\}|<\chi\max_{i=1,2,n=\tilde{n},\tilde{n}'}\{\text{Im}\{f_{p,n}^{(i)}\}\}$ provided that $|\text{Re}\{f_{p,n}^{(i)}-f_{p,\{\tilde{n},\tilde{n}'\}}^{(\{1,2\})}\}|>\chi\,\text{Im}\{f_{p,n}^{(i)}+f_{p,\{\tilde{n},\tilde{n}'\}}^{(\{1,2\})}\}$ for all $(\tilde{n},1)\neq(n,i)\neq(\tilde{n}',2)$. In the above, the parameter χ and the nonresonant component $\tilde{a}(f)$ have interpretations as in Sec. IV. Noting that $\tilde{a}(f)$ is approximately constant near $f_{p,\tilde{n}}^{(1)}$ and $f_{p,\tilde{n}'}^{(2)}$, i.e., that $\tilde{a}(f)\approx\tilde{a}(f_{p,\tilde{n}}^{(1)})\approx\tilde{a}(f_{p,\tilde{n}'}^{(2)})$, and combining it with the two pole contributions, $T(f)$ is recognized as having a pair of poles and zeros as shown in the second equality in (5). It follows that, depending on the locations of these zeros, the two maxima in graphs of $|T(f)|$ versus f for f

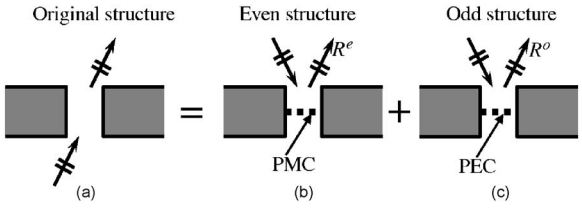

FIG. 6. Equivalent problems for symmetric structures.

$\approx \mathrm{Re}\{f^{(\{1,2\})}_{p,\{\tilde{n},\tilde{n}'\}}\}$ typically are accompanied by one or two deep minima.

To further dissect the above described *double resonance* enhanced transmission phenomenon, two cases are to be distinguished. Below, Sec. V A describes double resonance enhanced transmission phenomena occurring in symmetric structures, viz. structures with identical bottom and top slabs; these resonances only exist for $\tilde{n}=\tilde{n}'$. Sec. V B describes double resonance enhanced transmission phenomena in asymmetric structures; these may occur both when $\tilde{n}=\tilde{n}'$ and $\tilde{n}\neq\tilde{n}'$.

A. Symmetric structures—Identical top and bottom slabs

Assume that in the structure of Fig. 1 the top and bottom slabs are identical, that is $h_1=h_2$ and $\varepsilon_1=\varepsilon_2$; this implies that $f^{(1)}_{r,\tilde{n}}=f^{(2)}_{r,\tilde{n}}$ and $f^{(1)}_{p,\tilde{n}}\approx f^{(2)}_{p,\tilde{n}}$. It follows that the fields in the structure/excitation configuration of Fig. 1 can be expressed as a sum of fields whose electric field components tangential to the $z=0$ structural symmetry plane exhibit *even* and *odd* symmetry.[35,37] Specifically, fields in the original structure/field configuration in the $z>0$ (upper) half-space are the superposition of responses of the two structures in Figs. 6(b) and 6(c), obtained from the structure in Fig. 1 by inserting perfect magnetic and electric conductors in the symmetry plane $z=0$, to even and odd plane wave excitations. The transmission coefficient of the original structure can be expressed as $T(f)=[R^e(f)-R^o(f)]/2$, where $R^e(f)$ and $R^o(f)$ are electric field reflection coefficients of the structures in Figs. 6(b) and 6(c), respectively. This decomposition lends itself to several observations. First, it is noted that for $f\approx\mathrm{Re}\{f^{(1,2)}_{p,\tilde{n}}\}$, both $R^e(f)$ and $R^o(f)$ are characterized by a single pole; these poles are $f^{(1)}_{p,\tilde{n}}$ [for $R^e(f)$] and $f^{(2)}_{p,\tilde{n}}$ [for $R^o(f)$]. For $d=0$, the *odd* configuration degenerates into a grounded slab; as this structure supports no resonance only a *single* pole and enhanced transmission peak in $T(f)$ exists. For moderate $d\neq 0$ the *even* and *odd* configurations are sufficiently different leading to pole separations resulting in twin peaks in graphs of $|T(f)|$ versus f for $f\approx\mathrm{Re}\{f^{(\{1,2\})}_{p,\tilde{n}}\}$. For large d ($d>2s$), the *even* and *odd* configurations in Figs. 6(a) and 6(b) become essentially *identical* due to the evanescent nature of the field in the holes; this leads to almost *identical* poles $f^{(1)}_{p,\tilde{n}}$ and $f^{(2)}_{p,\tilde{n}}$ and a *single* enhanced transmission peak with decreased magnitude results. Next, since only a single propagating Floquet mode exists and the structures are lossless, $R^{e,o}(f)=e^{j\phi^{e,o}(f)}$ where $\phi^{e,o}(f)$ are real valued phase functions, which experience 2π variations as f passes near $\mathrm{Re}\{f^{(1,2)}_{p,\tilde{n}}\}$. The transmission coefficient thus can be expressed as $T(f)=je^{j[\phi^o(f)+\phi^e(f)]/2}\sin\{[\phi^o(f)-\phi^e(f)]/2\}$. It is concluded that *total* transmission results, i.e., $|T(f)|=1$, whenever $\phi^o(f)-\phi^e(f)=\pm\pi$. The latter condition is satisfied near distinct $f^{(1)}_{p,\tilde{n}}$ and $f^{(2)}_{p,\tilde{n}}$. Therefore, for lossless symmetric configurations, not just enhanced but *total* transmission is *guaranteed* through moderately thick plates ($d<2s$) and for f near $\mathrm{Re}\{f^{(\{1,2\})}_{p,\{\tilde{n},\tilde{n}'\}}\}$. Finally, the zeros $f^{(1)}_{z,\tilde{n}}$ and $f^{(2)}_{z,\tilde{n}}$ in (5) are comprised of a complex conjugate pair when $\phi^o(f)-\phi^e(f)\neq 0,2\pi$ for any real f whereas they are a real-valued pair when equation $\phi^o(f)-\phi^e(f)=0,2\pi$ has real solutions $f^{(1)}_{z,\tilde{n}}$ and $f^{(2)}_{z,\tilde{n}}$.

Figure 7 shows the evolution of TE poles $f^{(1,2)}_{p,-1}$, zeros $f^{(1,2)}_{z,-1}$ and residues $\mathrm{Res}\{T(f^{(1,2)}_{p,-1})\}$ as a function of d for $L_x=26$ mm, $L_y=5$ mm, $s=2.4$ mm, $\varepsilon_{1,2}=3$, $h_{1,2}=8$ mm and $\xi=0.1$. For moderate plate thicknesses d the poles $f^{(1,2)}_{p,-1}$ are distinct and the residues are $|\mathrm{Res}\{T(f^{(1,2)}_{p,-1})\}|\approx\mathrm{Im}\{f^{(1,2)}_{p,-1}\}$ leading to two strong peaks in $|T(f)|$. The zeros $f^{(1,2)}_{z,-1}$ comprise a complex conjugate pair leading to a minimum in $|T(f)|$. As d decreases, the pole $f^{(2)}_{p,-1}$ and both zeros $f^{(1,2)}_{p,-1}$ approach each other and merge on the real axis for $d=0$. As a result, for $d=0$ a *single* pole $f^{(1)}_{p,-1}$ and a real zero $f^{(1)}_{z,-1}$ are obtained. As d increases, the poles $f^{(1,2)}_{p,-1}$ approach one another and merge when $d\approx 2s$. For $d>2s$, $\mathrm{Res}\{T(f^{(1)}_{p,-1})\}\approx -\mathrm{Res}\{T(f^{(1)}_{p,-1})\}$ leading to a single transmission peak with reduced magnitude. As seen from the figure, the actual behavior of poles, zeros, and residues is in line with the above theoretical observations.

Figure 8 depicts $|T(f)|$ for the structure in Fig. 7 illuminated by a TE wave when $f\approx\mathrm{Re}\{f^{(1,2)}_{p,-1}\}$ for different d. For $d=0$, a *single* transmission peak is found followed by a real zero. For thicker plates, peak *double*, that is, a very narrow additional peak appears; at the peak maxima $|T(f)|=1$, i.e., *total* transmission is achieved. As the thickness increases the peaks approach each other and merge for sufficiently thick plates ($d=5$ mm). Transmission coefficients of even thicker plates exhibit to a *single* peak whose magnitude decreases exponentially with d. It is clear that the behavior of $|T(f)|$ agrees well with theoretical observations made above and the evolution of the poles, zeros, and residues in Fig. 7.

Figure 9 shows $V(d/h)$ for the structure in Figs. 7 and 8 for $d=1.5$ mm and f corresponding to the lower and higher maxima in Fig. 8. It is seen that $V(z/h)$ indeed has essentially odd and even symmetry due to the excitation of odd and even resonances.

B. Asymmetric structures—Different top and bottom slabs

Assume that in the structure of Fig. 1 the top and bottom slabs are different, that is $h_1\neq h_2$ *and/or* $\varepsilon_1\neq\varepsilon_2$, but the structure parameters are such that two resonant frequencies coincide, i.e., $f^{(1)}_{r,\tilde{n}}=f^{(2)}_{r,\tilde{n}'}$, resulting in $f^{(1)}_{p,\tilde{n}}\approx f^{(2)}_{p,\tilde{n}'}$. In general, this situation may occur for different ($\tilde{n}\neq\tilde{n}'$) or identical ($\tilde{n}=\tilde{n}'$) modal indices. If we were to lift the above restrictions on L_x and L_y, the resonances in the two slabs even

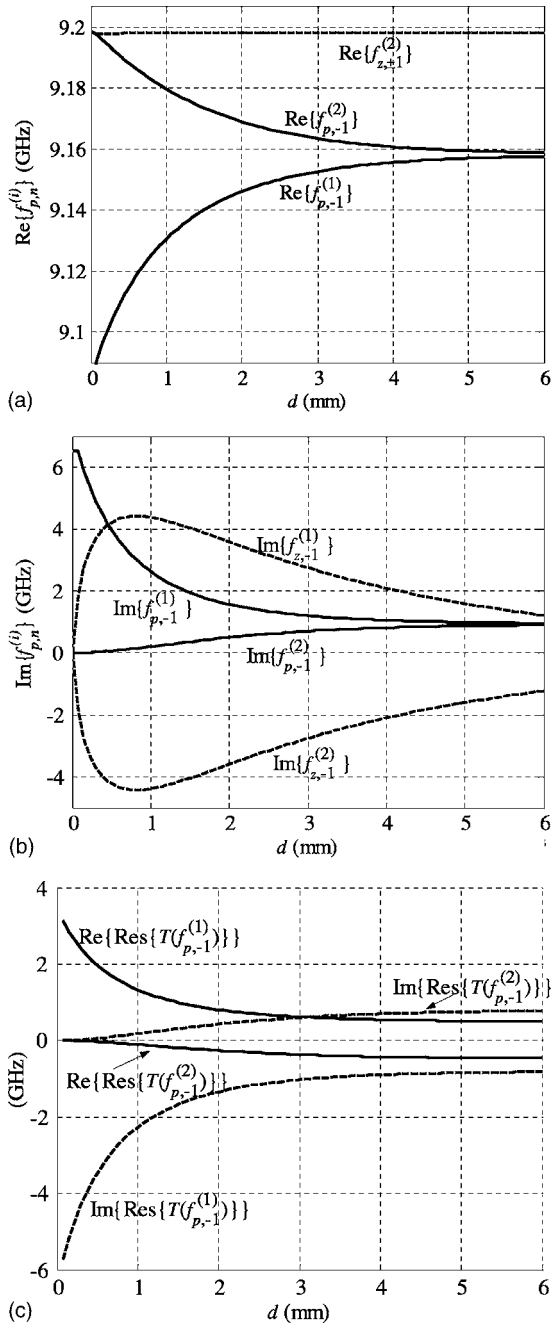

FIG. 7. TE poles, zeros and residues as a function of d for a symmetric structure with identical slabs. (a) $\mathrm{Re}\{f_{p,-1}^{(1,2)}\}$ and $\mathrm{Re}\{f_{z,-1}^{(1,2)}\}$; (b) $\mathrm{Im}\{f_{p,-1}^{(1,2)}\}$ and $\mathrm{Im}\{f_{z,-1}^{(1,2)}\}$; (c) $\mathrm{Re}\{\mathrm{Res}\{f_{p,-1}^{(1,2)}\}\}$ and $\mathrm{Im}\{\mathrm{Res}\{f_{p,-1}^{(1,2)}\}\}$. The structure parameters are $L_x=26$ mm, $L_y=5$ mm, $s=2.4$ mm, $\varepsilon_1=3$, $h_1=8$ mm and $\varepsilon_2=3$, $h_2=8$ mm, $\xi=0.1$.

could be associated with strong coupling between Floquet modes with transverse wave vectors pointing in different directions in the x-y plane. However, when abiding to these restrictions, and focusing on the structure and frequency range considered in Sec. III, only two cases remain: $\tilde{n}=-\tilde{n}'=\pm 1$ or $\tilde{n}=\tilde{n}'=\pm 1$. When $\tilde{n}=-\tilde{n}'=\pm 1$, the double resonance enhanced transmission is caused by strong coupling between the zeroth order Floquet mode and Floquet modes associated with GWs that travel along the plate in *opposite directions* through the top and bottom slabs; other Floquet modes also

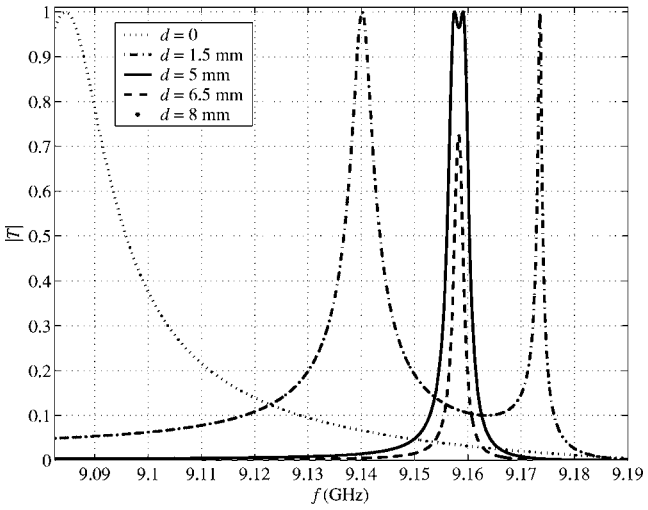

FIG. 8. TE transmission coefficient for the structure parameters in Fig. 7 and different d.

participate in these interactions but their influence is weaker. For example, for the structure giving rise to Fig. 2, this occurs near $\xi=0.2005$, i.e., when the trajectories of $\mathrm{Re}\{f_{p,-1}^{(1)}\}$ and $\mathrm{Re}\{f_{p,1}^{(2)}\}$ intersect. Note that such coupling is possible only in a very narrow ξ range since the trajectories of $\mathrm{Re}\{f_{p,\tilde{n}}^{(1)}\}$ and $\mathrm{Re}\{f_{p,\tilde{n}'}^{(2)}\}$ in dispersion graphs typically intersect at a substantial angle. When $\tilde{n}=\tilde{n}'=\pm 1$ the double resonance enhanced transmission is due to strong coupling between the zeroth order Floquet mode and the Floquet modes associated with GWs traveling in the *same direction* in two slabs but having a different field structure. Note that such coupling often is allowed for a relatively wide range of ξ since, in this case, the trajectories of $\mathrm{Re}\{f_{p,\tilde{n}}^{(1)}\}$ and $\mathrm{Re}\{f_{p,\tilde{n}'}^{(2)}\}$ typically intersect at a small angle.

Figure 10 shows the evolution of TM poles $f_{p,-1}^{(1)}$, $f_{p,1}^{(2)}$, zeros $f_{z,-1}^{(1)}$, $f_{z,1}^{(2)}$, and residues $\mathrm{Res}\{T(f_{p,-1}^{(1)})\}$, $\mathrm{Res}\{T(f_{p,1}^{(2)})\}$ as a function of d for the *asymmetric* structure with parameters of

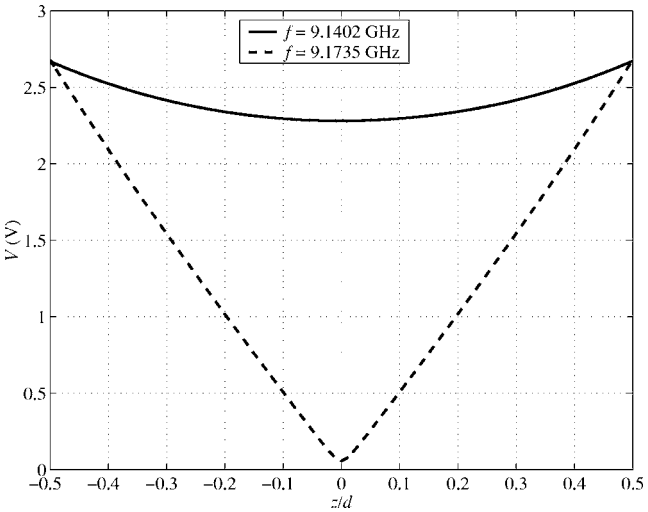

FIG. 9. Distribution of the field inside holes $V(z/d)$ under TE plane wave excitation. The structure parameters are as in Fig. 7 for $d=1.5$ mm.

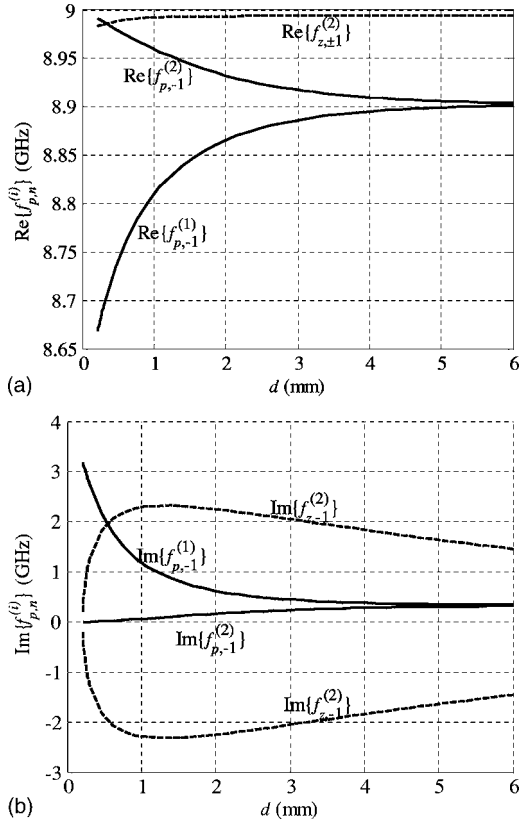

FIG. 10. TM poles and zeros as a function of d for an asymmetric structure with different slabs but under double resonance condition. (a) $\mathrm{Re}\{f_{p,-1}^{(1,2)}\}$ and $\mathrm{Re}\{f_{z,-1}^{(1,2)}\}$; (b) $\mathrm{Im}\{f_{p,-1}^{(1,2)}\}$ and $\mathrm{Im}\{f_{z,-1}^{(1,2)}\}$. The structure parameters are as in Fig. 2 and $\xi=0.2005$ is chosen on the intersection between $\mathrm{Re}\{f_{p,-1}^{(1)}\}$ and $\mathrm{Im}\{f_{p,1}^{(2)}\}$ in Fig. 2.

the structure leading to Fig. 2 and $\xi=0.2005$, i.e., at the intersection of the $\mathrm{Re}\{f_{p,-1}^{(1)}\}$ and $\mathrm{Re}\{f_{p,1}^{(2)}\}$ trajectories in Fig. 2(a). The behavior of the poles, zeros, and residues is similar to that in Fig. 7 for *symmetric* configurations. For instance, two poles and zeros are observed; for large d $(d>2s)$ the poles merge and $\mathrm{Res}\{T(f_{p,-1}^{(1)})\}\approx-\mathrm{Res}\{T(f_{p,-1}^{(1)})\}$; the zeros are comprised of a complex conjugate pair. However, the zeros and poles do not coincide as $d\to 0$; therefore two transmission peaks are obtained even for $d=0$.

Figure 11 shows the magnitude of the TM transmission coefficient for again the same structure aside from the thickness d. The behavior of $|T(f)|$ is similar to that in Fig. 7. For instance, *double* transmission peaks are obtained for moderately thick plates whereas only a *single* decreased peak is obtained for very thick plates. However, *total* transmission is not obtained, i.e., $|T(f)|$ never reaches unity. In addition, the second (narrower) transmission peak does not disappear as $d\to 0$. This is in agreement with the results in Fig. 10. Note that $|T(f)|$ is significantly increased compared to $|T(f)|$ in Figs. 3 and 5 describing the behavior of the same configuration but in the *single resonance* regime.

Figure 12 shows $V(d/h)$ in the structure of Fig. 11 for $d=1.5$ mm and f corresponding to the two maxima in Fig. 11. It is seen that $V(z/h)$ is large at both the top and bottom faces of the holes. This implies the existence of a combined resonance in both slabs.

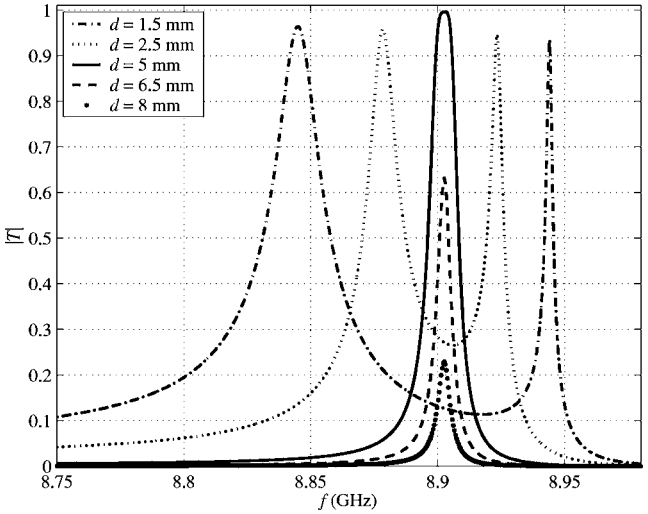

FIG. 11. TM transmission coefficient for different d. The structure is as in Fig. 10.

Finally, *double resonance* enhanced transmission is demonstrated when $\tilde{n}=\tilde{n}'=-1$. Figure 13 depicts the magnitude of TM transmission coefficient for $L_x=26$ mm, $L_y=5$ mm, $s=2.4$ mm, $\varepsilon_1=3$, $h_1=3$ mm and $\varepsilon_2=2.275$, $h_2=4$ mm, $\xi=0$. These structure parameters are chosen such that $f_{p,-1}^{(1)}$ and $f_{p,1}^{(2)}$ are close to each other. It is seen that again *double resonance* transmission is observed. The behavior of $|T(f)|$ is similar to that in Figs. 7 and 11. The behavior of poles, zeros, and residues is very similar to that in Fig. 10 and therefore is not shown.

VI. SUMMARY

Enhanced transmission through PEC plates perforated by small holes and sandwiched in between two dielectric slabs can be achieved in frequency bands where the incident plane wave couples to resonances supported by the perforated plate

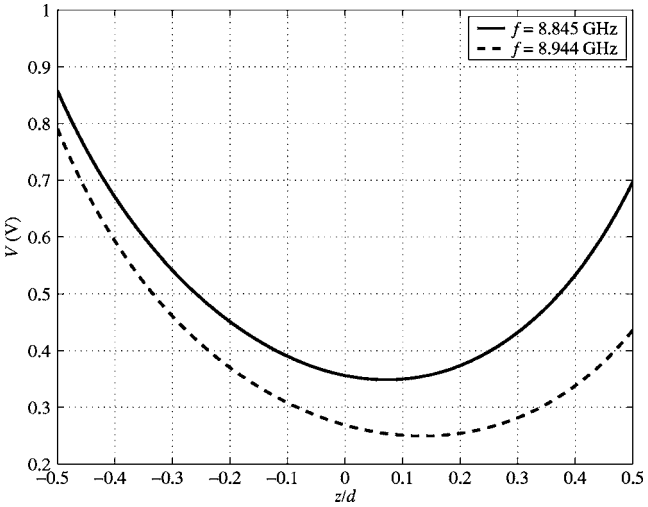

FIG. 12. Distribution of the field inside holes $V(z/d)$ under TM plane wave excitation. The structure parameters are as in Fig. 10 for $d=1.5$ mm.

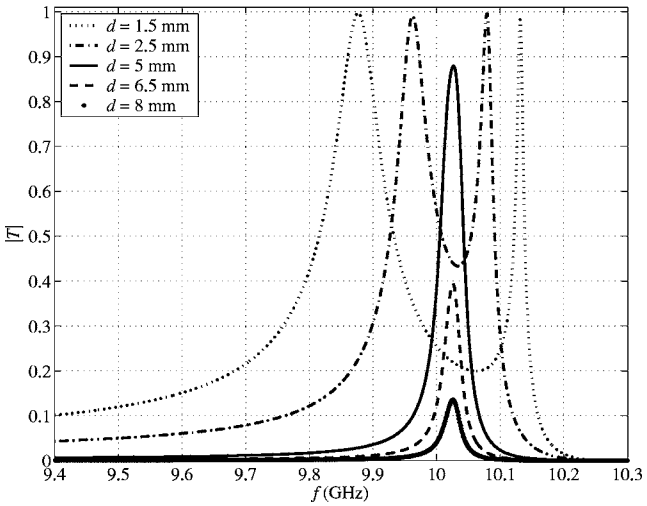

FIG. 13. TM transmission coefficient for different d. The structure parameters are L_x=26 mm, L_y=5 mm, s=2.4 mm, ε_1=3, h_1=3 mm and ε_2=2.275, h_2=4 mm, ξ=0.

that are associated with the existence of guided waves in grounded dielectric slabs. Approximations of the resonant frequencies can be obtained by matching the wave number of one of the Floquet modes generated by the periodic hole array to that of a grounded slab GW. The suggested structure allows enhanced transmission in the optical and the microwave regimes, and this for both transverse magnetically and electrically polarized incident fields. The existence of two distinct enhanced transmission regimes was demonstrated. In the single resonance regime the incident plane wave couples to a resonance in a single (top or bottom) slab. The transmission coefficient versus frequency graph exhibits a high peak though no total transmission is achieved; moreover the peak narrows, the position of its maximum shifts, and its magnitude exponentially decreases as the plate's thickness increases. In the double resonance regime the incident plane wave couples to resonances in both slabs. Such coupling leads to transmission peak doubling and, for thick plates, to a significant increase in the maximum transmission allowed (compared to the single resonance regime). Changes in the nature of the enhanced transmission phenomenon when transitioning from infinitesimally thin to very thick perforated plates were studied. It was shown that for thin plates one peak significantly narrows compared to the other one and eventually disappears. For moderately thick plates two transmission peaks of equal size appear. For very thick plates the two peaks merge, resulting in one peak with reduced magnitude. Double resonances may appear for symmetric as well as for asymmetric structures. It was demonstrated that for symmetric lossless structures, *total* transmission with two peaks is guaranteed for moderately thick plates and any angle of incidence. The two peaks are associated with odd and even resonances. For asymmetric structures, special conditions on the period and slab parameters must be satisfied to ensure the existence of a double resonance.

Note that nothing prevents the transmission enhancement mechanism studied in this paper from occurring in concert with those associated with surface waves supported by perforated plates[21,27,36] and SPPs;[6–19] in fact, all enhanced transmission phenomena occurring on these structures are manifestations of the same physics, i.e., coupling between the incident plane wave and resonances supported by the perforated plates that are associated with slow waves. This implies significant flexibility in the design of periodic structures exhibiting enhanced transmission phenomena. Studies into the effect of losses in the perforated plate and dielectric slabs are ongoing. These losses are expected to be smaller than those resulting from SPP-based enhanced transmission mechanisms since in the former the GWs are distributed in the entire volume of the dielectric and are not confined to a metal surface. Slab and plate losses, however, may lead to a quantitative decrease in magnitude and qualitative change in the shape/(dis)appearance of the enhanced transmission peaks. The structures and phenomena explored in this paper may find uses in near-field imaging, target identification, and the construction of antennas, tunable filters, mode converters, and amplifiers.

ACKNOWLEDGMENTS

This research was supported by DARPA VET Program under AFOSR Contract No. F49620-01-1-0228. We would like to thank an anonymous reviewer for his/her helpful comments.

*Author to whom correspondence should be addressed. Email address: vitaliy@emlab.uiuc.edu

[1] P. Sandoz, R. Giust, and G. Tribillon, Opt. Commun. **161**, 197 (1999).

[2] P. F. Goldsmith, *Quasioptical Systems-Gaussian Beam, Quasioptical Propagation, and Applications* (Wiley IEEE Press, Hoboken, NJ, 1998).

[3] IEEE Trans. Electromagn. Compat. **30** (3) (1988).

[4] H. A. Bethe, Phys. Rev. **66**, 163 (1944).

[5] T. W. Ebbesen, H. J. Lezec, H. F. Ghaemi, T. Thio, and P. A. Wolff, Nature (London) **391**, 667 (1998).

[6] S. Enoch, E. Popov, M. Neviere, and R. Reinisch, J. Opt. A, Pure Appl. Opt. **4**, S83 (2002).

[7] D. E. Grupp, H. J. Lezec, T. W. Ebbesen, K. M. Pellerin, and T. Thio, Appl. Phys. Lett. **77**, 1569 (2000).

[8] A. Krishman, T. Thio, T. J. Kim, H. J. Lezec, T. W. Ebbesen, P. A. Wolff, J. Pendry, L. Martin-Moreno, and J. J. Garcia-Vidal, Opt. Commun. **200**, 1 (2001).

[9] E. Popov, M. Neviere, S. Enoch, and R. Reinisch, Phys. Rev. B **62**, 16100 (2000).

[10] T. Thio, H. J. Lezec, T. W. Ebbesen, K. M. Pellerin, G. D. Lewen, A. Nahata, and R. A. Linke, Nanotechnology **13**, 429 (2002).

[11] M. M. J. Treacy, Phys. Rev. B **66**, 195105 (2002).

[12] A. Degiron, H. J. Lezec, W. L. Barnes, and T. W. Ebbesen, Appl.

Phys. Lett. **81**, 4327 (2002).
[13] L. Martín-Moreno, F. J. García-Vidal, H. J. Lezec, K. M. Pellerin, T. Thio, J. B. Pendry, and T. W. Ebbesen, Phys. Rev. Lett. **86**, 1114 (2001).
[14] S. A. Darmanyan and A. V. Zayats, Phys. Rev. B **67**, 035424 (2003).
[15] M. Sarrazin, J. P. Vigneron, and J. M. Vigoureux, Phys. Rev. B **67**, 085415 (2003).
[16] D. R. Jackson, T. Zhao, J. T. Williams, and A. A. Oliner, *2003 IEEE International Symposium on Antennas and Propagation: URSI North American Radio Science Meeting, 22–27 June 2003* (IEEE, Columbus, OH, 2003), Vol. 2, p. 1095.
[17] A. A. Oliner and D. R. Jackson, *2003 IEEE International Symposium on Antennas and Propagation: URSI North American Radio Science Meeting, 22–27 June 2003* (IEEE, Columbus, OH, 2003), Vol. 2, p. 1091.
[18] T. Thio, K. M. Pellerin, R. A. Linke, H. J. Lezec, and T. W. Ebbesen, Opt. Lett. **26**, 1972 (2001).
[19] F. I. Baida, D. Van Lebeke, and B. Guizal, Appl. Opt. **42**, 6811 (2003).
[20] H. Raether, *Surface Plasmons on Smooth and Rough Surfaces and on Gratings* (Springer-Verlag, Berlin, 1988).
[21] V. Lomakin, N. W. Chen, S. Q. Li, and E. Michielssen, IEEE Microw. Wirel. Compon. Lett. **14**, 355 (2004).
[22] J. A. Porto, F. J. García-Vidal, and J. B. Pendry, Phys. Rev. Lett. **83**, 2845 (1999).
[23] P. Lalanne, J. P. Hugonin, S. Astilean, M. Palamaru, and K. D. Moller, J. Opt. A, Pure Appl. Opt. **2**, 48 (2000).
[24] Q. Cao and P. Lalanne, Phys. Rev. Lett. **88**, 057403 (2002).
[25] S. Astilean, P. Lalanne, and M. Palamaru, Opt. Commun. **175**, 265 (2000).
[26] A. Hessel and A. A. Oliner, Appl. Opt. **4**, 1275 (1965).
[27] V. Lomakin, N. W. Chen, and E. Michielssen, *IEEE AP-S Symposium and Radio Science Meeting*, Columbus, OH (2003).
[28] L. Martin-Moreno, F. J. Garcia-Vidal, H. J. Lezec, A. Degiron, and T. W. Ebbesen, Phys. Rev. Lett. **90**, 167401 (2003).
[29] F. J. Garcia-Vidal, L. Martin-Moreno, H. J. Lezec, and T. W. Ebbesen, Appl. Phys. Lett. **83**, 4500 (2003).
[30] M. Beruete, F. Falcone, M. Sorolla, I. Campillo, J. S. Dolado, L. Martín-Moreno, and F. J. García-Vidal, *2004 IEEE AP-S International Symposium and USNC/URSI National Radio Science Meeting* (2004).
[31] A. P. Hibbins, J. R. Sambles, C. R. Lawrence, and J. R. Brown, Phys. Rev. Lett. **92**, 143904 (2004).
[32] D. Qu, D. Grischkowsky, and W. Zhang, Opt. Lett. **29**, 896 (2004).
[33] H. Cao and A. Nahata, Opt. Express 12 (2004).
[34] C. C. Chen, IEEE Trans. Microwave Theory Tech. **19**, 475 (1971).
[35] C.-C. Chen, IEEE Trans. Microwave Theory Tech. **21**, 1 (1973).
[36] V. Lomakin, N. W. Chen, and E. Michielssen, *Progress in Electromagnetics Research Symposium*, Honolulu, Hawaii (2003).
[37] R. E. Collin, *Field Theory of Guided Waves* (IEEE Press, Piscataway, NJ, 1991).
[38] The nonresonant component $a(f)$ experiences rapid variations near branch frequencies $f_{b,n}=(nc)[\mathrm{sign}(n)-\xi]^{-1}L_x^{-1}$ appearing in $T(f)$; these frequencies often are termed Rayleigh frequencies and are associated with Rayleigh-Wood anomalies. When a pole $f_{p,\tilde{n}}^{(\tilde{i})}$ and a branch point $f_{b,\tilde{n}'}$ reside close to each other, then they simultaneously affect the behavior of $T(f)$.